Published in final edited form as:
Nat Struct Mol Biol. 2015 January ; 22(1): 50–56. doi:10.1038/nsmb.2935.

A coiled-coil domain acts as a molecular ruler in LPS chain length regulation

Gregor Hagelueken[#1,2], **Bradley R. Clarke**[#3], **Hexian Huang**[#1], **Anne Tuukkanen**[4], **Iulia Danciu**[4,5], **Dmitri I. Svergun**[4], **Rohanah Hussain**[6], **Huanting Liu**[1], **Chris Whitfield**[3,*], and **James H. Naismith**[1,*]

[1]Biomedical Sciences Research Complex, University of St Andrews, St Andrews, Fife, KY16 9ST, UK

[2]Institute for Physical and Theoretical Chemistry, University of Bonn, Wegelerstr. 12, 53115 Bonn, Germany

[3]Department of Molecular and Cellular Biology, University of Guelph, Guelph, Ontario, N1G 2W1, Canada

[4]European Molecular Biology Laboratory, Hamburg Outstation, Notkestraße 85, 22603 Hamburg, Germany

[6]Diamond Light Source, Didcot, OX11 0QX, UK

[#] These authors contributed equally to this work.

Abstract

Long-chain bacterial polysaccharides play important roles in pathogenicity. In *Escherichia coli* O9a, a model for ABC transporter dependent polysaccharide assembly, a large extracellular carbohydrate with a narrow distribution of size is polymerized from monosaccharides by a complex of two proteins, WbdA (polymerase) and WbdD (terminating protein). Such careful control of polymerization is recurring theme in biology. Combining crystallography and small angle X-ray scattering, we show that the C-terminal domain of WbdD contains an extended coiled-coil that physically separates WbdA from the catalytic domain of WbdD. The effects of insertions and deletions within the coiled-coil region were analyzed *in vivo*, revealing that polymer size is controlled by varying the length of the coiled-coil domain. Thus, the coiled-coil domain of WbdD functions as a molecular ruler that, along with WbdA:WbdD stoichiometry, controls the chain length of a model bacterial polysaccharide.

[*]naismith@st-andrews.ac.uk; cwhitfie@uoguelph.ca.
[5]Present address: Gregor Mendel Institute for Molecular Plant Biology GmbH, Dr. Bohr-Gasse 3, 1030 Vienna, Austria

Author contributions: GH, HH, JHN carried out the crystallography; AT, ID, DS carried out SAXS experiments, data analysis and modelling; BRC, HL, CW carried out mutagenesis and *in vivo* work; HH, RH carried out CD experiments; All authors analysed data and contributed to writing the paper.

Accession codes: The SAXS data and models of WbdD$^{1\text{-}459}$ and WbdD$^{1\text{-}556}$ are deposited in the Small-Angle Scattering Biological Data Bank (www.sasbdb.org), entries SASDAH6 and SASDAJ6, respectively. The crystallographic data are available from the Protein Data Bank (www.pdb.org) entry 4uw0.

Europe PMC Funders Author Manuscripts

Europe PMC Funders Author Manuscripts

Introduction

Lipopolysaccharide (LPS) is a major constituent of the outer membrane of Gram-negative bacteria. In most cases, its presence is essential for cell viability and in addition LPS plays important roles in pathogenicity. LPS is composed of a conserved membrane anchor molecule, lipid A (endotoxin), and a short conserved core oligosaccharide that links lipid A to an immunogenic O-antigen polysaccharide of variable length [1,2]. The carbohydrate composition and size of the O antigen is hyper-variable with more than 180 variants described in *E. coli* strains alone [3]. The O-antigen is among the first molecules encountered by the host during infection and it has been shown to be vital in protecting pathogenic bacteria from the host-immune response by avoiding complement mediated killing [4]. A fascinating structural feature of most O antigens is that their chain lengths fall within defined ranges (termed the 'modal distribution') that are O-serotype dependent (Figure 1A). Such exquisite control of polymerization is a recurring theme in biology (e.g. phage tails or the length of injection needles in type-III-secretion-systems[5,6]) but its origin is generally poorly understood at a structural and molecular level, even where the identities of the protein components from the assembly systems are known.

There are three recognized bacterial polysaccharide biosynthesis pathways that produce O-antigen glycans (the Wzy dependent-, the ATP-binding cassette (ABC) transporter dependent- and the synthase dependent pathway) [1]. The components that determine the modal distributions of O-antigen glycans vary in these biosynthesis pathways but none of the processes are fully understood at a molecular level. This study focuses the assembly of the serotype O9a antigen from on *E. coli*, a well-characterized prototype of the ABC transporter-dependent pathway.

The O9a glycan chain is synthesized in the cytoplasm using an undecaprenyl diphosphate carrier molecule. The chain is extended by addition of mannose residues to the non-reducing terminus and glycan chain length is terminated by the addition of a phosphomethyl moiety that blocks further chain extension [7] (Figure 1B). Elongation of the polymannose O9a-antigen is performed by WbdA, whose two glycosyltransferase (GT) domains cooperate in a distributive reaction mechanism to produce a glycan composed of alternating pairs of α-(1→2)- and α-(1→3)-linked mannoses in a tetrasaccharide repeat unit [8,9] (Figure 1B). The N-terminal domain of WbdA is predicted to catalyse formation of the α-(1→2) linkage and the C-terminal domain the α-(1→3) linkage; both domains belong to the glycosyl transferase family 4 [9]. The overall structure of WbdA and the positioning of the two catalytic sites relative to one another have not been reported. Chain termination is catalyzed by WbdD, (a kinase and methyltranferase) that adds a terminal phosphomethyl moiety at the O3 position of the terminal mannose residue halting further chain extension [10-12] (Figure 1B). The terminating phosphomethyl modification is recognized by a specific carbohydrate binding module forming part of the ABC transporter, giving an elegant quality control method to ensure only (completed) glycans of the desired length are exported and assembled into LPS [13,14]. WbdD is a membrane-associated protein and its interaction with WbdA is essential for the ability of the otherwise soluble polymerase to act on the membrane-embedded undecaprenyl lipid-linked acceptor [11]. Full-length WbdD (708 residues) is membrane bound and forms aggregates, which has precluded *in vitro* studies of the complex.

Only WbdD constructs truncated at residue 556 (WbdD$^{1-556}$) or 459(WbdD$^{1-459}$), thus lacking both WbdA and membrane interacting regions, have been crystallized[15]. The structure of WbdD$^{1-556}$ revealed a trimer, in which each monomer is comprized of a methyltransferase domain, followed by kinase domain followed by a 12 residue helix; residues beyond 470 were disorderd and thus not seen in the electron density[15]. The short 12 residue helix forms a trimeric bundle with the same helix in two other monomers around a three fold axis, giving the overall structure the appearance of an umbrella[15]. WbdD$^{1-459}$ lacks the helix and exists as a monomer.

Mathematical modelling has been used in an effort to understand the molecular basis for the observed modality of the O9a glycan [16]. This resulted in a "variable geometry model", in which the stoichiometry of the WbdA:WbdD complex is a crucial factor regulating modal length and size distribution of the polymer. Perturbing expression of WbdA or WbdD to alter the stoichiometry altered chain lengths and distribution in a manner predicted by the model [16]. However, in addition to complex stoichiometry, the mathematical model requires a measuring element (hereafter referred to as a molecular ruler). In this study, we set to define the molecular ruler. We demonstrate that the C-terminus of WbdD forms an extended coiled-coil and that this structural feature acts as a central element of the required molecular ruler that together with complex stoichiometry defines the size of the O9a glycan. This is the first complete molecular and structural description of such a polymerisation system.

Results

Extended X-ray structure of the C-terminal helix-bundle WbdD$^{1-556}$

As we had reported previously, WbdD truncated beyond residue 459 (WbdD$^{1-459}$) gave a monomeric protein that crystallized well but possessed severely reduced kinase activity. The latter was unexpected, since both catalytic domains were left intact [17]. A second truncated construct, WbdD$^{1-556}$, produced active trimeric protein that gave cubic crystals which were refractory to optimization and diffracted to resolutions between 4 and 8 Å. We reported that a dehydration of these crystals gave a 2.2 Å resolution structure with a monomer in the asymmetric unit. In this crystal structure only a poorly defined C-terminal poly-alanine helix (that forms a helical bundle) comprising residues 459 to 473 (approximately) was built, precluding analysis of the C-terminal domain[15].

For this work, we evaluated 10 datasets obtained from non-dehydrated crystals on the hypothesis[15] that the dehydration itself was responsible for disordering of the C-terminus. One WbdD$^{1-556}$ crystal diffracted to 3.9 Å and the C-terminal domain up to residue 505 was clearly visible in the electron density, following deformable elastic network (DEN) refinement [18]. Only 51 residues remained disordered in the resulting structure (Table 1). The newly traced residues adopted a helical arrangement generating an extended C-terminal helix to which sequence was assigned (Figure 2A, B). The extended helix forms a coiled-coil arrangement via the crystallographic three-fold axis. Furthermore, this coiled-coil domain interacts with the kinase active site, resulting in the ordering of two previously disordered active site loops (αQ-αR, residues 398-416 and α16-βQ, residues 377-381, the "activation" loop). These two loops interact with each other via a π-stacking interaction between W408 and W382 (Figure 2B). We had previously obtained weak but interpretable

density for two mannose residues at the kinase active site[15], this newly ordered structure completes the kinase catalytic site (Figure 2B), supplies residues to recognize the substrate (consistent with site directed mutagenesis)[15], and rationalizes the role of the C-terminus in kinase activity[15].

The structure of the C-terminal coiled-coil domain in WbdD

Small-angle X-ray scattering (SAXS) data were collected for the WbdD$^{1-459}$, WbdD$^{1-556}$ and WbdD$^{1-600}$ constructs (Figure 3A). WbdD$^{1-600}$ behaved as an aggregated assembly in gel filtration and its SAXS data were uninterpretable. The scattering from WbdD$^{1-459}$ yielded a molecular mass (MM) estimate of 52±5 kDa (Table 2) in agreement with the calculated molecular mass (MM) of the monomer (49kDa). The reconstructed *ab initio* model of WbdD$^{1-459}$ fits the SAXS data with discrepancy $\chi = 0.9$ and matches well with the crystallographic monomer[15] (Supplementary Figure 1).

The MM estimate of WbdD$^{1-556}$ from SAXS (MM = 165±20 kDa, Table 2) indicates a trimeric assembly of this construct, in agreement with gel filtration and crystallography[15]. The *ab initio* WbdD$^{1-556}$ model (imposing P3 symmetry) reveals a mushroom-like particle that resembles the crystal structure (Figure 3B,C). The trimeric arrangement of the catalytic domains of WbdD$^{1-556}$ corresponds to the head of the mushroom and the coiled-coil partly matches its stalk. In the *ab initio* model, the stalk is clearly longer than that in the crystal structure (Figures 3B, C), indicating that the coiled-coil extends further than is currently resolved by crystallography. The theoretical scattering, computed from the crystallographic model at 3.9 Å where residues from 506 to 556 are missing, provides a poor fit to the SAXS data from WbdD$^{1-556}$ with $\chi = 4.8$ (Figure 3A, green curve).

Sequence analysis using the COILS algorithm [19] predicts that residues 460-600 of WbdD (and 460-556 of WbdD$^{1-556}$) form a coiled-coil structure (Supplementary Figure 2). When the new structure (Figure 3B) was analysed by the CCCP server [20], residues 462-505 gave an average coiled-coil radius of 8.5 Å with a 1.42 Å rise-per-residue of the coiled-coil axis (Supplementary Table 1, TWISTER [21] an alternative program gave similar values, radius: 8.4 Å, rise per residue: 1.42 Å/residue). Using these experimental parameters, we built a model of the complete coiled-coil of WbdD$^{1-556}$ using the CCBuilder server [22], leading to a coiled-coil of ~135 Å in total length. The hybrid structure (X-ray structure of N-terminal domains plus model of coiled-coil) has an improved fit to the SAXS scattering ($\chi = 3.3$ vs 4.8) compared to just the residues of the X-ray model. Rigid body refinement with SASREF was employed and the angle of catalytic domains relative to coiled-coil was allowed to move [23]. Precedent for such movement was seen in the various crystal structures[15,17] which have different angles with a more closed cap seen at higher resolution consistent with tighter packing. The angle between the catalytic domains and the coiled-coil in the SASREF model opened by ~5° resulting in a χ value of 1.29 (Figure 3A). Figure 3C shows that this refined rigid-body molecular model of WbdD$^{1-556}$ fits very well the shape of the *ab initio* SAXS model (which is bulkier as the solvation shell is visible in SAXS). Circular dichroism analysis using the CONTINLL algorithm[24] (via Dichroweb [25]) on spectra collected on B23 at Diamond of WbdD$^{1-459}$ and WbdD$^{1-556}$ confirms a detectable increase in helical content as expected for the addition of a coiled-coil (Supplementary Figure S3). The good fit

between experimental and model structures encouraged us to extrapolate our model to include the additional 44 residues (predicted to be coiled-coil). By this approach the coiled-coil of full-length WbdD is predicted to be around 200 Å.

Insertions and deletions in the coiled-coil affect polysaccharide length

The length of the coiled-coil was experimentally modulated by insertion or deletion of residues within this structure. To minimize stoichiometry changes in the WbdA:WbdD complex[16] resulting from mutations in WbdD perturbing its expression level, an experimental system was used in which modified His_6-WbdD proteins were expressed from the same transcript (and promoter) as WbdA-Flag in an *E. coli wbdD wbdA* deletion mutant (CWG917). This experimental test system gives a polymer with a modal length of 11 repeat units; slightly shorter than the 14 observed in the native O9a product. Four consecutive heptads were deleted within the coiled-coil region of WbdD (Fig 3A, Δ(GHIJ)), amino acids 558-585). Expression of the Δ(GHIJ) derivative in CWG917 resulted in LPS with a shorter average O-PS chain length compared to the modal length obtained with the wild-type His_6-WbdD (Fig 3B and C). Deletion of an additional heptad (Fig 3A, Δ(GHIJK), amino acids 558-592) caused a further reduction by one repeat unit in the O-PS (Fig 3, B and C). A His_6-WbdD derivative containing a coiled-coil domain extended by insertion of two additional blocks of heptads CDEF (i.e. amino acids 466-507) designated $(CDEF)_2$ (Fig 3A) produced a polymer with a longer average O-PS chain length (Fig 3 B and C). A longer coiled-coil insertion $(ABCDEF)_2$ was also constructed, the O-PS synthesized was longer than the native product but not within error longer than that observed from the $(CDEF)_2$ derivative, indicating there is a limit to the extension possible. Since full length protein was refractory to structural analysis, we made two insertion and two deletion variants of $WbdD^{1\text{-}556}$ in order to gain some structural insight into the effect of the changes in the coiled-coil region. CD spectroscopy (Supplementary Figure S3) was used to characterize constructs $WbdD^{1\text{-}459}$, $WbdD^{1\text{-}556}$, $WbdD^{1\text{-}556}(CDEF)_2$, $WbdD^{1\text{-}556}(ABCDEF)_2$, $WbdD^{1\text{-}556}$(ΔGHIJK) and $WbdD^{1\text{-}556}$(ΔGHIJ). Although the presence of aggregates (which hinders precise concentration estimation) means we treat the numbers with caution, we do observe a correlation between predicted and observed changes in helical content (Supplementary Figure S3). SAXS data on these constructs also showed that solutions of these proteins contain aggregates that render detailed analysis impossible (as seen for $WbdD^{1\text{-}600}$).

Previous work has shown that the chain-length of the O9a antigen can be manipulated by altering the levels of expression of either WbdA or WbdD [16]. To determine whether altered stoichiometry could explain the results with the coiled-coil variants, the relative amounts of His_6-WbdD and WbdA-Flag were quantitated from the whole-cell lysates by Western immunoblotting using anti-His and anti-Flag antibodies [16]. The WbdD:WbdA ratios for the strains containing His_6-WbdD(ΔGHIJK) and (ΔGHIJ) were approximately 1.3 and 1.7-fold lower, respectively than the ratio observed for the wild type His_6-WbdD. However, these changes in stoichiometry would tend to generate a longer polymer, rather than the observed shorter products [16]. The $WbdD(CDEF)_2$:WbdA ratio was 1.5-fold higher than that that observed with wild type His_6-WbdD which would tend to yield a shorter polymer, opposite to the observed products [16]. Thus, in each of these cases, the change in stoichiometry would

operate counter to the experimental observation and we can conclude that changes in polymer length are due to the change in the protein structure, rather than altered stoichiometry. However, the ratio of WbdD(ABCDEF)$_2$:WbdA was 2.5-fold lower than that of the wild type and thus possible that the increase in O-PS chain length in this mutant was due to decreased expression of WbdD(ABCDEF)$_2$ relative to WbdA. To determine whether a 2.5-fold decrease in WbdD expression could affect the chain length to the extent observed for WbdD(ABCDEF)$_2$, the expression level of plasmid-encoded wild type His$_6$-WbdD was titrated relative to constitutively expressed endogenous WbdA. The LPS chain-length was examined by SDS-PAGE and the His$_6$-WbdD levels were quantitated by Western immunoblotting. From this analysis it was determined that a 2.5-fold decrease in WbdD(ABCDEF)$_2$ relative to WbdA was insufficient to cause the observed O-PS chain length increase (Supplementary Figure S4). As a final control for mutant function, we confirmed that dramatic changes in stoichiometry in complexes containing the WbdD constructs with altered coiled-coils reproduced the size-distribution shifts (for one insertion and one deletion) observed for the native protein [16] (Supplementary Figure S5).

Discussion

The concept that biology can control the length of polymeric structures by means of a 'molecular ruler' dates back to the observation that the lengths of bacteriophage tail structures are narrowly distributed [26]. Since then, molecular rulers have been identified in other polymerization systems [27]. In principle, a molecular ruler is a protein, or a domain of a protein-protein complex, whose size defines the length of a polymeric structure by terminating polymerisation when the nascent polymer reaches the requisite length [27]. Well studied examples include the phage-λ tail system, which involves two proteins gpH (the ruler) and gpU (the terminator)[5], flagellar hooks in *Salmonella* [28,29] using FliK and YscP and type-three secretion system needles in *Yersinia* [6,30-32]. Although these systems have been thoroughly characterized at a genetic level, detailed molecular descriptions of the ruler have been lacking. Polymerisation control but of a different sort is also seen in the Cas10•Csn ribonucleoprotein complex from the CRISPR system[33], where multiple copies of Csm3 protein bind the nascent oligonucleotide and each additional copy of Csm3 results in a 6-nucleotide increment.

An explicit factor in the mathematical model [16] developed to explain chain length regulation in *E. coli* O9a LPS system is the presence of a molecular ruler separating WbdA and WbdD. The rigid coiled-coil domain of WbdD is the obvious candidate for this ruler. The coiled-coil is at the C-terminus and effectively separates the kinase (capping reaction) from WbdA (the polymerase), which interacts with the C-terminus of WbdD [12]. WbdA has two active sites at which the undecaprenol diphosphate anchored polymer is elongated by addition of carbohydrate monomers. Coiled-coils have been shown to act as rigid spacers in other non-polymerization based systems: e.g. tetherin [34] or type-I restriction modification enzymes [35,36]. The 92 kDa gpH ruler protein from the phage-λ ruler system [5] has a predicted coiled-coil [19], although the coiled-coil has not been experimentally investigated.

The GLYCAM server (www.glycam.org) calculates the length of a repeat unit of the O9a *E. coli* carbohydrate polymer to be ~15 Å, meaning 14 repeating units will be around 210 Å

(Figure 4A). This is close to the 200 Å length of the coiled-coil in WbdD calculated from our crystallographic and modelling data. We suggest that the polymer grows at WbdA by switching between the two mannosyltransferase active sites in this two-domain protein [9] until long enough to reach and be capped by the kinase domain of WbdD (which is held by the coiled-coil domain at around 200 Å from the WbdA) (Figure 5). Direct experimental assessment of a reconstituted WbdD: WbdA complex has not been possible as purified full length WbdD aggregates. Instead we tested our hypothesis by engineering WbdD with coiled-coil domains with shorter and longer lengths. We deleted 28 and 35 residues (multiples of 7 were used to conserve the heptad register), corresponding to 40 Å (2 repeat units) and 50 Å (3 repeat units) respectively (Figure 4A). *In vivo* data shows the resulting polymers produced in these mutants are indeed progressively shorter (Figure 4 B,C). Insertions of 56 residues (80 Å increase; five repeats) and 84 residues (120 Å increase; nine repeats) (Figure 4A) both give O-polysaccharides with chain lengths longer than that of the wild type. Taken together the *in vitro* data establish the direct relationship between coiled-coil domain length and LPS polymer length required for a molecular ruler (Figure 4B,C, 5, S5). The close correlation between a physical length and sequence of coiled-coil structures may make them particularly suited as molecular rulers for biological systems more generally.

The bifunctional kinase-methyltransferase WbdD component is identical in *E. coli* serotypes O9 and O9a, the difference in O antigens arises to due to changes in linkage geometry catalysed by the differing WbdAs[37]. O antigens and biosynthesis systems similar to *E. coli* O9 are also found in *Klebsiella pneumoniae* [37] and *Hafnia alvei* [38]. A polymannose O antigen with a trisaccharide repeat unit is produced by *E. coli* serotype O8 (identical to *K. pneumoniae* O5). It possesses a WbdA protein with 3 mannosyltransferase domains [9] and the cognate WbdD protein only possesses the methyltransferase activity but the coiled-coil domain is conserved (Supplementary Figure 6) [10]. Consequently we suggest a similar ruler mechanism is operative in each of these polymannose O antigen systems. An ABC transporter-dependent process is also used by *Geobacillus stearothermophilus*, where the S-layer glycoprotein carries O-linked poly-D-rhamnose glycans capped with methyl groups[39]. Interestingly the organization of the system differs, as there is no separate terminating methyltransferase protein. Instead the methyltransferase is part of a multidomain protein that includes one of the glycosyltransferases required for chain extension. Importantly, the methyltransferase and glycosyltransferase domains are separated by a region of predicted coiled-coil structure (Supplementary Figure S6) and we predict this region may function as the ruler. An analogous situation may occur in biosynthesis of the O12 antigen in *K. pneumoniae* O12 and a related O-antigen structure in *Raoutella terrigena* [40,41], where terminal capping is achieved by addition of a β-linked 3-deoxy-D-*manno*-oct-2-ulosonic acid (Kdo) residue. In this multidomain protein, the putative Kdo transferase domain is separated from two chain extension glycosyltransferase domains by a region of coiled-coil structure (Supplementary Figure S6).

To our knowledge, the coiled-coil domain of WbdD represents the first molecular ruler characterized at a molecular level and we have shown that the ruler can be engineered by genetic modification to produce both longer and shorter carbohydrate polymers. The ease of

the genetic manipulation that can be used to tune the property of polymer may be another positive facet of coiled-coils as molecular rulers in nature but maybe also for chemical applications.

Online Methods

Protein expression & production

The procedures used for the cloning, expression and purification of WbdD$^{1-600}$, WbdD$^{1-556}$ and WbdD$^{1-459}$ have been described previously[15,17].

Crystallography

WbdD$^{1-556}$ was crystallized as previously reported[17]. Before flash cooling in liquid nitrogen, crystals were cryo-protected by transfer into a solution consisting of 1 µl ADP (5 mM), 0.5 µl magnesium chloride (100 mM), 3 µl glycerol and 6 µl mother liquor (0.13 M lithium sulfate; 0.10 M Tris-HCl pH 8.52; 1.18 M ammonium sulfate). A 3.9 Å diffraction data set was collected (λ = 0.9173 Å) using synchrotron beamline IO4-1 at the Diamond synchrotron (Didcot, UK). The data set was processed using XIA2 [43] and the structure was solved by molecular replacement (PHASER, [44]), using the WbdD$^{1-459}$ structure as search model (PDB-ID: 4AZW) [15]. The program gave a clear solution with a translation function Z-score of 30.9. Using deformable elastic network refinement [45] and jellybody refinement as implemented in REFMAC [46], the molecular replacement solution could be refined to R/R_{free}-factors of 26.8/34.1 and a model for the C-terminal helix could be build up to residue 498. The geometry of the model was analysed with MOLPROBITY [47] and was placed overall in the 91st centile (Molprobity Score: 2.90/ 91st percentile; Molprobity Clashscore: 30.1/ 83rd percentile). Ramachandran statistics were also calculated with MOLPROBITY (favoured: 83.0 %, outliers: 3.6 %). The data collection and refinement statistics are listed in Table 1, the coordinates are available from the RCSB with code 4uw0.

SAXS

SAXS measurements were carried out at beamline X33 (EMBL-DESY, Hamburg) at the DORIS III storage ring using a Pilatus 1M detector (Dectris) [48]. Purified WbdD constructs ([1-459] (C380S mutant), [1-556] and [1-600]) were measured at four different concentrations (1, 2, 5 and 10 mg/ml) in 20 mM BisTris pH 7, 50 mM NaCl, 5 mM DTT. For each measurement eight 15 s frames were collected and averaged. No substantial changes of the scattering intensity were detected during the successive exposures indicating the absence of radiation damage. At the sample-detector distance of 2.7 m and a wavelength of λ = 1.5 Å the momentum transfer range of $0.01 < s < 0.6$ Å^{-1} was covered ($s = 4\pi \sin\theta/\lambda$, where 2θ is the scattering angle). The program PRIMUS [49]. was used to correct the data for buffer contribution, scale for solute concentration, and extrapolate the data to infinite solute dilution [49]. The statistics of the SAXS data collection are presented in Table 2. Data were reduced by automated radial averaging [50]. The radius of gyration R_g and the forward scattering intensity *I(0)*, were determined using Guinier analysis [51] and the indirect Fourier transformation using *GNOM* [52]. The latter program was employed to evaluate the maximum particle dimension D_{max} and the pair-distance distribution function $p(r)$. The molecular mass (MM_{SAXS}) of the protein constructs was calculated by comparison of the extrapolated

forward scattering with that from a reference bovine serum albumin (BSA) sample (MM_{ref} = 66 kDa). The excluded volume of the hydrated protein V_p was obtained with *DATPOROD* [53] providing an independent estimate of the molecular mass (MM_{POROD}). For globular proteins, hydrated protein volumes in Å^3 are about 1.7 times the molecular masses in Da.

SAXS modelling—Theoretical scattering profiles from the high-resolution models were calculated by *CRYSOL* [54]. *Ab initio* models of the WbdD$^{1-459}$ mutant and WbdD$^{1-556}$ constructs were obtained from the scattering data using the bead-modeling program *DAMMIN* [55]. An average of 10 independent reconstructions was used to generate a representative model by SUPCOMB [56] and *DAMAVER* [57]. Rigid-body modeling against the SAXS data was done using SASREF [23] to search for the optimum configuration of the N-terminal and C-terminal domains to minimize the discrepancy χ^2 between the experimental and computed SAXS data. The complete coiled-coil of WbdD$^{1-556}$ built using CCBuilder server [22] was modelled as a single entity.

CD measurements—CD experiments were performed using a nitrogen-flushed Module B end-station spectrophotometer at B23 Synchrotron Radiation CD Beamline at the Diamond Light Source, Oxfordshire, UK [58,5960]. Samples were typically prepared in 30 mM NaPi and 50mM NaF, pH 7.0. Measurements were carried out at 20 °C with sample concentration of 0.3mg/ml with 0.02cm pathlength cell using average amino acid molecular weight of 113. The data was processed using B23 CDApps (http://www.diamond.ac.uk/Beamlines/Soft-Condensed-Matter/B23/manual/Beamline-software.html).

Site-directed mutagenesis of WbdD and in vivo O-PS chain length analysis

The coiled-coil domain insertion ((CDEF)$_2$, (ABCDEF)$_2$) and deletion (Δ(GHIJK), Δ(GHIJ)) mutants were constructed by PCR based mutagenesis [61] using the primers described in Supplementary Table 2 with pWQ470 (His$_6$-WbdD) [11] as the template. To generate mutant plasmids encoding His$_6$-WbdDΔ(GHIJK) and Δ(GHIJ) two different forward primers (DELGJSPEF and DELGKSPEF, respectively), were used together with the same reverse primer (DELGKCOMR). Plasmids encoding the insertion mutants His$_6$-WbdD(CDEF)$_2$ and His$_6$-WbdD(ABCDEF)$_2$ were generated using the primer pairs, INS2XEFR/INS2XEFF, INSCDEFR/INSCDEFF and INSATOFR/ INSATOFF, respectively. The resulting mutants were sequenced and protein expression of these mutants was verified by western immunoblotting.

Wild-type and mutant His$_6$-WbdD constructs were cloned immediately upstream of a derivative of the *wbdA* gene (coding for a WbdA-Flag fusion protein) creating the same organization that occurs in the chromosomal locus and were expressed under the control of the L-arabinose-inducible P_{BAD} promoter. The His$_6$-WbdD and WbdA-Flag fusion proteins were expressed contiguously to provide consistent stoichiometry of the overexpressed proteins across individual experiments. Pwo DNA polymerase was used to amplify the *wbdA* gene from genomic *E. coli* O9a DNA from strain CWG28 [62], using the primers, WbdABgFw and WbdARv. The WbdARv primer contained sequence coding for a C-terminal Flag epitope tag. EcoRI and BglII restriction endonuclease sites (underlined) were incorporated into the forward primer and used with the blunt end formed at the 3′ end of the

PCR product for subsequent ligation reactions. The PCR product was digested with EcoRI and then ligated into EcoRI-SmaI-digested pWQ589 [8] to form pWQ457. Genes encoding the His_6-WbdD derivatives were amplified by PCR using primers, WBBDDHF1 and WbdDBg708. The amplification product was digested with EcoRI-BglII and ligated into EcoRI-BglII-cut pWQ457 to give, pWQ458 (wildtype His-WbdD), pWQ468 (Δ(GHIJK)), pWQ459 (Δ(GHIJ)), pWQ460 ($(CDEF)_2$), and pWQ469 ($(ABCDEF)_2$), respectively (Supplementary Table 2). To overexpress His_6-WbdD and the mutant derivatives together with WbdA-Flag, an *E. coli* O9a *wbdD wbdA* deletion mutant (CWG917)[11] was transformed with the relevant plasmid and grown for 16 h at 37° C in 5 mL of LB broth containing kanamycin (Km, 50 μg/mL) and glucose (0.4% w/v). The cultures were then diluted 1:100 into 5 mL of LB broth containing Km (50 μg/mL), D-mannose (0.1% w/v), and L-arabinose (0.01% w/v) and grown at 37° C until A_{600nm} values of 0.4-0.7 were reached. Three biological replicates were grown for each transformed strain. A volume equivalent to 1 A_{600nm} unit of each culture was collected by centrifugation at 12,000 × *g* for 1 min. Cells were lysed in 0.1 mL of SDS-PAGE loading buffer. LPS was analysed by treating one half of each sample with proteinase K [63] followed by SDS-PAGE in Tris-glycine buffer (Laemmli) and visualization by silver staining [64].

Proteins were analysed by Western immunoblotting using the remaining half of the lysed samples. Following SDS-PAGE, proteins were transferred to nitrocellulose membranes (Protran, PerkinElmer). Duplicate membranes were incubated with either anti-Penta-His antibody (Qiagen cat no 34660; used at a 1:1000 dilution)), or with anti-Flag M2 antibody (Sigma cat no F1804; used at a 1:1000 dilution) for detection of His_6-WbdD derivatives and WbdA-Flag, respectively. Horseradish peroxidase-conjugated goat anti-mouse secondary antibody (Jackson ImmunoResearch Laboratories cat no 115-036-003; used at a 1:3000 dilution) was used together with Luminata Classico Western HRP Substrate (Millipore) for protein detection. Validation and specificity information for the antibodies is found in the manufacturers literature. Immunoblot data was collected with a BioRad Chemidoc XRS system and Image processing was performed with ImageJ [42] to quantify the proteins by densitometry. For each mutant derivative, the mean pixel density ratio derived from the anti-His and the anti-Flag signals, respectively, was compared to the mean ratio derived from strains expressing the wildtype WbdD. To control for differences due to Western blot exposure times, wildtype and mutant signals were only compared among samples on the same blot.

Supplementary Material

Refer to Web version on PubMed Central for supplementary material.

Acknowledgements

This work is supported by Wellcome Trust Grant 081862 (JHN and CW); Senior Investigator Award WT100209MA (JHN), Natural Sciences, Engineering Research Council of Canada (CW) and the German Federal Ministry of Education and Research (BMBF) project BioSCAT, contract no: 05K12YE1 (AT and DIS). JHN is a Royal Society Wolfson Merit Award Holder and CW is a recipient of a Canada Research Chair. We are grateful for beamtime on beamlines B23 and IO4 at Diamond (Didcot, UK).

References

1. Raetz CRH, Whitfield C. Lipopolysaccharide endotoxins. Annu. Rev. Biochem. 2002; 71:635–700. [PubMed: 12045108]
2. Whitfield C, Trent MS. Biosynthesis and export of bacterial lipopolysaccharides. Annu. Rev. Biochem. 2014; 83:99–128. [PubMed: 24580642]
3. Stenutz R, Weintraub A, Widmalm G. The structures of Escherichia coli O-polysaccharide antigens. FEMS Microbiol. Rev. 2006; 30:382–403. [PubMed: 16594963]
4. Joiner KA. Complement evasion by bacteria and parasites. Annu. Rev. Microbiol. 1988; 42:201–230. [PubMed: 3059994]
5. Katsura I. Mechanism of length determination in bacteriophage lambda tails. Adv. Biophys. 1990; 26:1–18. [PubMed: 2150582]
6. Journet L, Agrain C, Broz P, Cornelis GR. The needle length of bacterial injectisomes is determined by a molecular ruler. Science. 2003; 302:1757–1760. [PubMed: 14657497]
7. Greenfield LK, Whitfield C. Synthesis of lipopolysaccharide O-antigens by ABC transporter-dependent pathways. Carbohydr. Res. 2012; 356:12–24. [PubMed: 22475157]
8. Greenfield LK, et al. Biosynthesis of the polymannose lipopolysaccharide O antigens from Escherichia coli serotypes O8 and O9a requires a unique combination of single- and multi-active site mannosyltransferases. J. Biol. Chem. 2012; 287:35078–35091. [PubMed: 22875852]
9. Greenfield LK, et al. Domain organization of the polymerizing mannosyltransferases involved in synthesis of the Escherichia coli O8 and O9a lipopolysaccharide O-antigens. J. Biol. Chem. 2012; 287:38135–38149. [PubMed: 22989876]
10. Clarke BR, Cuthbertson L, Whitfield C. Nonreducing Terminal Modifications Determine the Chain Length of Polymannose O Antigens of Escherichia coli and Couple Chain Termination to Polymer Export via an ATP-binding Cassette Transporter. J. Biol. Chem. 2004; 279:35709–35718. [PubMed: 15184370]
11. Clarke BR, Greenfield LK, Bouwman C, Whitfield C. Coordination of polymerization, chain termination, and export in assembly of the Escherichia coli lipopolysaccharide O9a antigen in an ATP-binding cassette transporter-dependent pathway. J. Biol. Chem. 2009; 284:30662–30672. [PubMed: 19734145]
12. Clarke BR, et al. In vitro reconstruction of the chain termination reaction in biosynthesis of the Escherichia coli O9a O-polysaccharide: the chain-length regulator, WbdD, catalyzes the addition of methyl phosphate to the non-reducing terminus of the growing glycan. J. Biol. Chem. 2011; 286:41391–41401. [PubMed: 21990359]
13. Cuthbertson L, Kimber MS, Whitfield C. Substrate binding by a bacterial ABC transporter involved in polysaccharide export. Proc. Natl. Acad. Sci. U.S.A. 2007; 104:19529–19534. [PubMed: 18032609]
14. Cuthbertson L, Mainprize IL, Naismith JH, Whitfield C. Pivotal roles of the outer membrane polysaccharide export and polysaccharide copolymerase protein families in export of extracellular polysaccharides in gram-negative bacteria. Microbiol. Mol. Biol. Rev. 2009; 73:155–177. [PubMed: 19258536]
15. Hagelueken G, et al. Structure of WbdD: a bifunctional kinase and methyltransferase that regulates the chain length of the O antigen in Escherichia coli O9a. Mol. Microbiol. 2012; 86:730–742. [PubMed: 22970759]
16. King JD, Berry S, Clarke BR, Morris RJ, Whitfield C. Lipopolysaccharide O antigen size distribution is determined by a chain extension complex of variable stoichiometry in Escherichia coli O9a. PNAS. 2014; 111:6407–6412. [PubMed: 24733938]
17. Hagelueken G, et al. Crystallization, dehydration and experimental phasing of WbdD, a bifunctional kinase and methyltransferase from Escherichia coli O9a. Acta Crystallogr D Biol Crystallogr. 2012; 68:1371–1379. [PubMed: 22993091]
18. Schröder GF, Levitt M, Brunger AT. Super-resolution biomolecular crystallography with low-resolution data. Nature. 2010; 464:1218–1222. [PubMed: 20376006]
19. Lupas, AN.; Gruber, M. The Structure of α-Helical Coiled Coils. Vol. 70. Elsevier; 2005. p. 37-38.

20. Grigoryan G, DeGrado WF. Probing Designability via a Generalized Model of Helical Bundle Geometry. J. Mol. Biol. 2011; 405:1079–1100. [PubMed: 20932976]
21. Strelkov SV, Burkhard P. Analysis of α-Helical Coiled Coils with the Program TWISTER Reveals a Structural Mechanism for Stutter Compensation. J. Struct. Biol. 2002; 137:54–64. [PubMed: 12064933]
22. Wood CW, et al. CCBuilder: an interactive web-based tool for building, designing and assessing coiled-coil protein assemblies. Bioinformatics. 2014; 30:3029–3035. [PubMed: 25064570]
23. Petoukhov MV, Svergun DI. Global Rigid Body Modeling of Macromolecular Complexes against Small-Angle Scattering Data. Biophys. J. 2005; 89:1237–1250. [PubMed: 15923225]
24. van Stokkum IH, Spoelder HJ, Bloemendal M, van Grondelle R, Groen FC. Estimation of protein secondary structure and error analysis from circular dichroism spectra. Anal. Biochem. 1990; 191:110–118. [PubMed: 2077933]
25. Sreerama N, Woody RW. Estimation of protein secondary structure from circular dichroism spectra: comparison of CONTIN, SELCON, and CDSSTR methods with an expanded reference set. Analytical Biochemistry. 2000; 287:252–260. [PubMed: 11112271]
26. King J. Bacteriophage T4 tail assembly: four steps in core formation. J. Mol. Biol. 1971; 58:693–709. [PubMed: 4933424]
27. Marshall WF. Cellular length control systems. Annu. Rev. Cell Dev. Biol. 2004; 20:677–693. [PubMed: 15473856]
28. Makishima S, Komoriya K, Yamaguchi S, Aizawa S-I. Length of the Flagellar Hook and the Capacity of the Type III Export Apparatus. Science. 2001; 291:2411–2413. [PubMed: 11264537]
29. Erhardt M, Singer HM, Wee DH, Keener JP, Hughes KT. An infrequent molecular ruler controls flagellar hook length in Salmonella enterica. EMBO J. 2011; 30:2948–2961. [PubMed: 21654632]
30. Agrain C, Sorg I, Paroz C, Cornelis GR. Secretion of YscP from Yersinia enterocolitica is essential to control the length of the injectisome needle but not to change the type III secretion substrate specificity. Mol. Microbiol. 2005; 57:1415–1427. [PubMed: 16102009]
31. Wagner S, Stenta M, Metzger LC, Dal Peraro M, Cornelis GR. Length control of the injectisome needle requires only one molecule of Yop secretion protein P (YscP). Proc. Natl. Acad. Sci. U.S.A. 2010; 107:13860–13865. [PubMed: 20643949]
32. Wagner S, et al. The helical content of the YscP molecular ruler determines the length of the Yersinia injectisome. Mol. Microbiol. 2009; 71:692–701. [PubMed: 19055526]
33. Hatoum-Aslan A, Samai P, Maniv I, Jiang W, Marraffini LA. A Ruler Protein in a Complex for Antiviral Defense Determines the Length of Small Interfering CRISPR RNAs. J. Biol. Chem. 2013; 288:27888–27897. [PubMed: 23935102]
34. Hinz A, et al. Structural basis of HIV-1 tethering to membranes by the BST-2/tetherin ectodomain. Cell Host Microbe. 2010; 7:314–323. [PubMed: 20399176]
35. Kim J-S, et al. Crystal structure of DNA sequence specificity subunit of a type I restriction-modification enzyme and its functional implications. Proc. Natl. Acad. Sci. U.S.A. 2005; 102:3248–3253. [PubMed: 15728358]
36. Price C, Lingner J, Bickle TA, Firman K, Glover SW. Basis for changes in DNA recognition by the EcoR124 and EcoR124/3 type I DNA restriction and modification enzymes. J. Mol. Biol. 1989; 205:115–125. [PubMed: 2784505]
37. Kido N, Sugiyama T, Yokochi T, Kobayashi H, Okawa Y. Synthesis of Escherichia coli O9a polysaccharide requires the participation of two domains of WbdA, a mannosyltransferase encoded within the wb* gene cluster. Mol. Microbiol. 1998; 27:1213–1221. [PubMed: 9570406]
38. Kubler-Kielb J, Whitfield C, Katzenellenbogen E, Vinogradov E. Identification of the methyl phosphate substituent at the non-reducing terminal mannose residue of the O-specific polysaccharides of Klebsiella pneumoniae O3, Hafnia alvei PCM 1223 and Escherichia coli O9/O9a LPS. Carbohydr. Res. 2012; 347:186–188. [PubMed: 22169179]
39. Steiner K, et al. Molecular Basis of S-layer Glycoprotein Glycan Biosynthesis in Geobacillus stearothermophilus. J. Biol. Chem. 2008; 283:21120–21133. [PubMed: 18515358]
40. Vinogradov E, et al. Structures of lipopolysaccharides from Klebsiella pneumoniae. Eluicidation of the structure of the linkage region between core and polysaccharide O chain and identification of

the residues at the non-reducing termini of the O chains. J. Biol. Chem. 2002; 277:25070–25081. [PubMed: 11986326]

41. Mertens K, et al. Antiserum against Raoultella terrigena ATCC 33257 identifies a large number of Raoultella and Klebsiella clinical isolates as serotype O12. Innate Immunity. 2010; 16:366–380. [PubMed: 20053705]
42. Abràmoff MD, Magalhães PJ, Ram SJ. Image processing with ImageJ. Biophotonics International. 2004; 11:36–42.

Additional References for Online Methods

43. Winter G. xia2: an expert system for macromolecular crystallography data reduction. J. Appl. Crystallogr. 2010; 43:186–190.
44. McCoy AJ, et al. Phasercrystallographic software. J. Appl. Crystallogr. 2007; 40:658–674. [PubMed: 19461840]
45. Schröder GF, Levitt M, Brunger AT. Super-resolution biomolecular crystallography with low-resolution data. Nature. 2010; 464:1218–1222. [PubMed: 20376006]
46. Nicholls RA, Long F, Murshudov GN. Low-resolution refinement tools in REFMAC5. Acta Crystallogr. D Biol. Crystallogr. 2012; 68:404–417. [PubMed: 22505260]
47. Chen VB, et al. MolProbity: all-atom structure validation for macromolecular crystallography. Acta Crystallogr. D Biol. Crystallogr. 2010; 66:12–21. [PubMed: 20057044]
48. Roessle MW, et al. Upgrade of the small-angle X-ray scattering beamline X33 at the European Molecular Biology Laboratory, Hamburg. J. Appl. Crystallogr. 2007; 40:190–194.
49. Konarev PV, Volkov VV, Sokolova AV, Koch MHJ, Svergun DI. PRIMUS: a Windows PC-based system for small-angle scattering data analysis. J. Appl. Crystallogr. 2003; 36:1277–1282.
50. Petoukhov MV, Konarev PV, Kikhney AG, Svergun DI. ATSAS2.1 – towards automated and web-supported small-angle scattering data analysis. J. Appl. Crystallogr. 2007; 40:s223–s228.
51. Guinier A. La diffraction des rayons X aux tres petits angles: applications a l'etude de phenomenes ultramicroscopiques. Annales de physique. 1939; 12:161–237.
52. Svergun DI. Determination of the regularization parameter in indirect-transform methods using perceptual criteria. J. Appl. Crystallogr. 1992; 25:495–503.
53. Petoukhov MV, et al. New developments in the ATSAS program package for small-angle scattering data analysis. J. Appl. Crystallogr. 2012; 45:342–350. [PubMed: 25484842]
54. Svergun D, Barberato C, Koch MHJ. CRYSOL– a Program to Evaluate X-ray Solution Scattering of Biological Macromolecules from Atomic Coordinates. J. Appl. Crystallogr. 1995; 28:768–773.
55. Svergun DI. Restoring low resolution structure of biological macromolecules from solution scattering using simulated annealing. Biophys J. 1999; 76:2879–2886. [PubMed: 10354416]
56. Kozin MB, Svergun DI. Automated matching of high- and low-resolution structural models. J. Appl. Crystallogr. 2001; 34:33–41.
57. Volkov VV, Svergun DI. Uniqueness of ab initio shape determination in small-angle scattering. J. Appl. Crystallogr. 2003; 36:860–864.
58. Jávorfi T, Hussain R, Myatt D, Siligardi G. Measuring circular dichroism in a capillary cell using the b23 synchrotron radiation CD beamline at diamond light source. Chirality. 2010; 22(Suppl 1):E149–53. [PubMed: 21038386]
59. Hussain, R.; Jávorfi, T.; Siligardi, G. Comprehensive Chirality. Elsevier; 2012. p. 438-448.doi: 10.1016/B978-0-08-095167-6.00841-7
60. Hussain R, Jávorfi T, Siligardi G. Circular dichroism beamline B23 at the Diamond Light Source. J Synchrotron Radiat. 2012; 19:132–135. [PubMed: 22186655]
61. Liu H, Naismith JH. An efficient one-step site-directed deletion, insertion, single and multiple-site plasmid mutagenesis protocol. BMC Biotechnol. 2008; 8:91. [PubMed: 19055817]
62. Whitfield C, Schoenhals G, Graham L. Mutants of Escherichia coli O9: K30 with Altered Synthesis and Expression of the Capsular K30 Antigen. Microbiology. 1989; 135:2589–2599.

63. Hitchcock PJ, Brown TM. Morphological heterogeneity among Salmonella lipopolysaccharide chemotypes in silver-stained polyacrylamide gels. J. Bacteriol. 1983; 154:269–277. [PubMed: 6187729]

64. Tsai CM, Frasch CE. A sensitive silver stain for detecting lipopolysaccharides in polyacrylamide gels. Anal. Biochem. 1982; 119:115–119. [PubMed: 6176137]

Europe PMC Funders Author Manuscripts

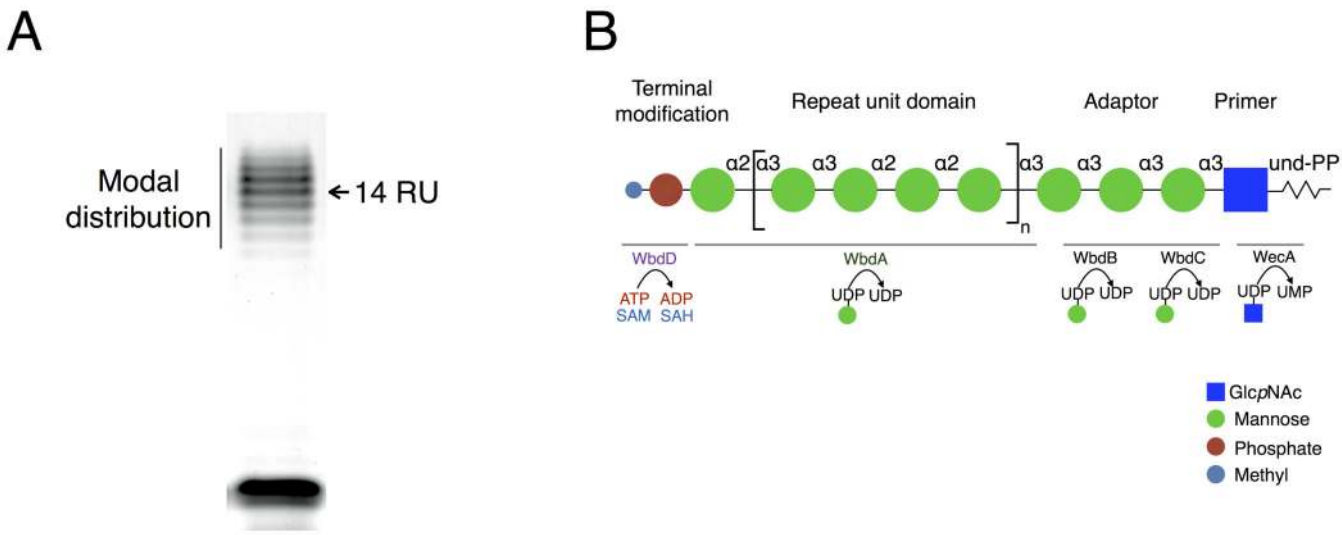

Figure 1.

A) Silver stained SDS-PAGE of wild type *E. coli* O9 LPS, illustrating the modal size distribution with an average length of 14 repeating units (RU). The data are reproduced from a previous study[16]. **B)** Schematic view of the biosynthesis of O9a polymer. The polymer contains a repeating tetrasaccharide (RU) and is built as an undecaprenol diphosphate (Und-PP)-linked intermediate by 3 mannosyltransferases, including the polymerizing enzyme WbdA. The N-terminal domain of WbdA catalyzes formation of the α-(1→2) linkage and the C-terminal domain is predicted to form the α-(1→3) linkages. Polymerisation is terminated by WbdD which caps the polymer by phosphorylating then methylating the terminal mannose and the resulting molecule is exported by the ABC transporter before ligation to lipid A-core.

Europe PMC Funders Author Manuscripts

Europe PMC Funders Author Manuscripts

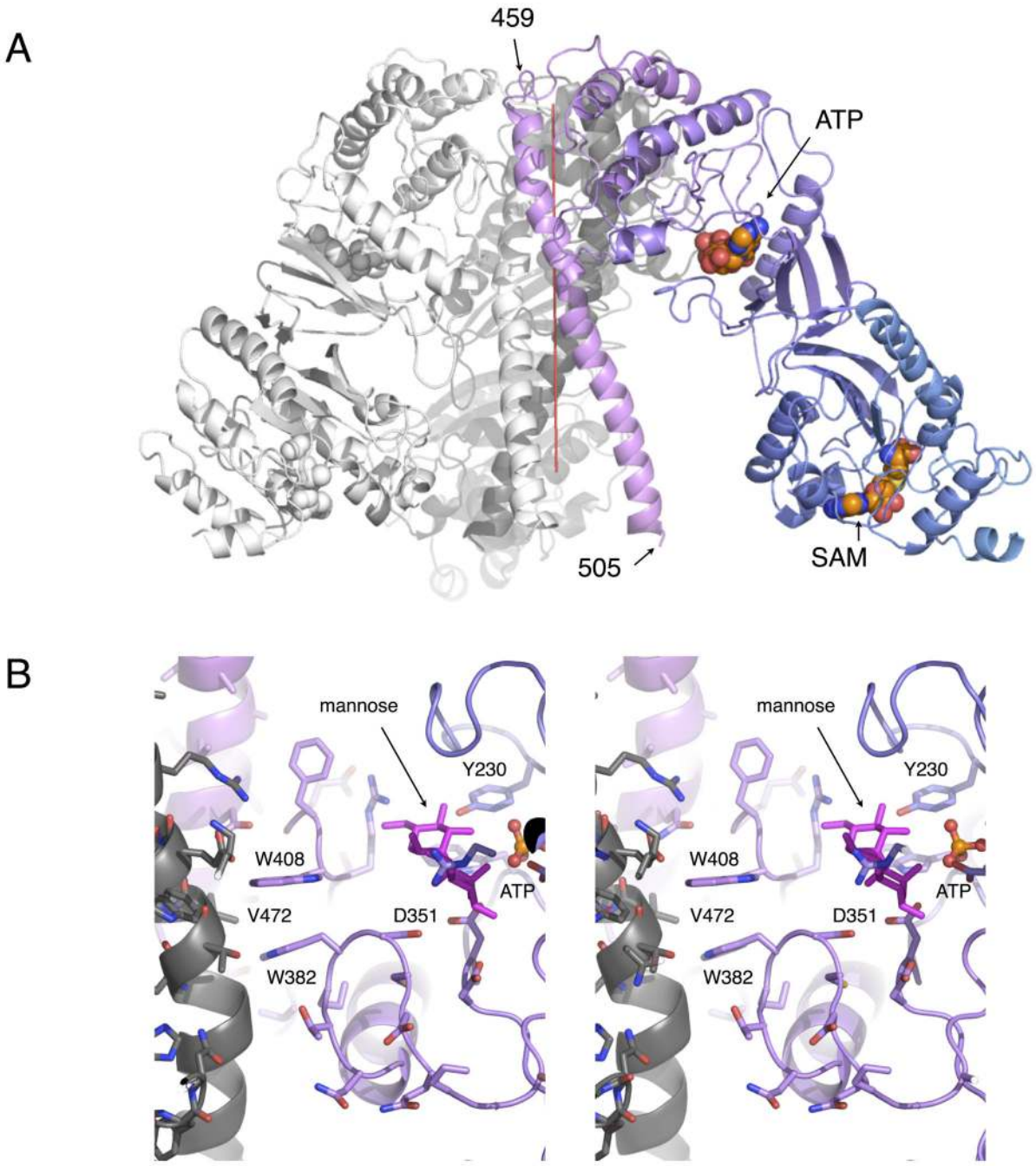

Figure 2.

A) 3.9 Å X-ray structure of WbdD$^{1\text{-}556}$, the trimer is shown in cartoon representation. One monomer is colored with a gradient running from blue (N-terminus) to pink (C-terminus). Spheres represent the nucleotides in the catalytic domains. The trimer axis is drawn as a red line. Arrows mark the start- and end-point of the coiled-coil. **B)** Interaction of the coiled-coil domain with the active site of WbdD (stereo pair). The color scheme is identical to C. Selected residues are numbered and shown as sticks. The cofactor ATP is shown as ball-

and-stick model. The mannose (purple) is from a superimposed model of the WbdD$^{1\text{-}459}$ structure [15].

Europe PMC Funders Author Manuscripts

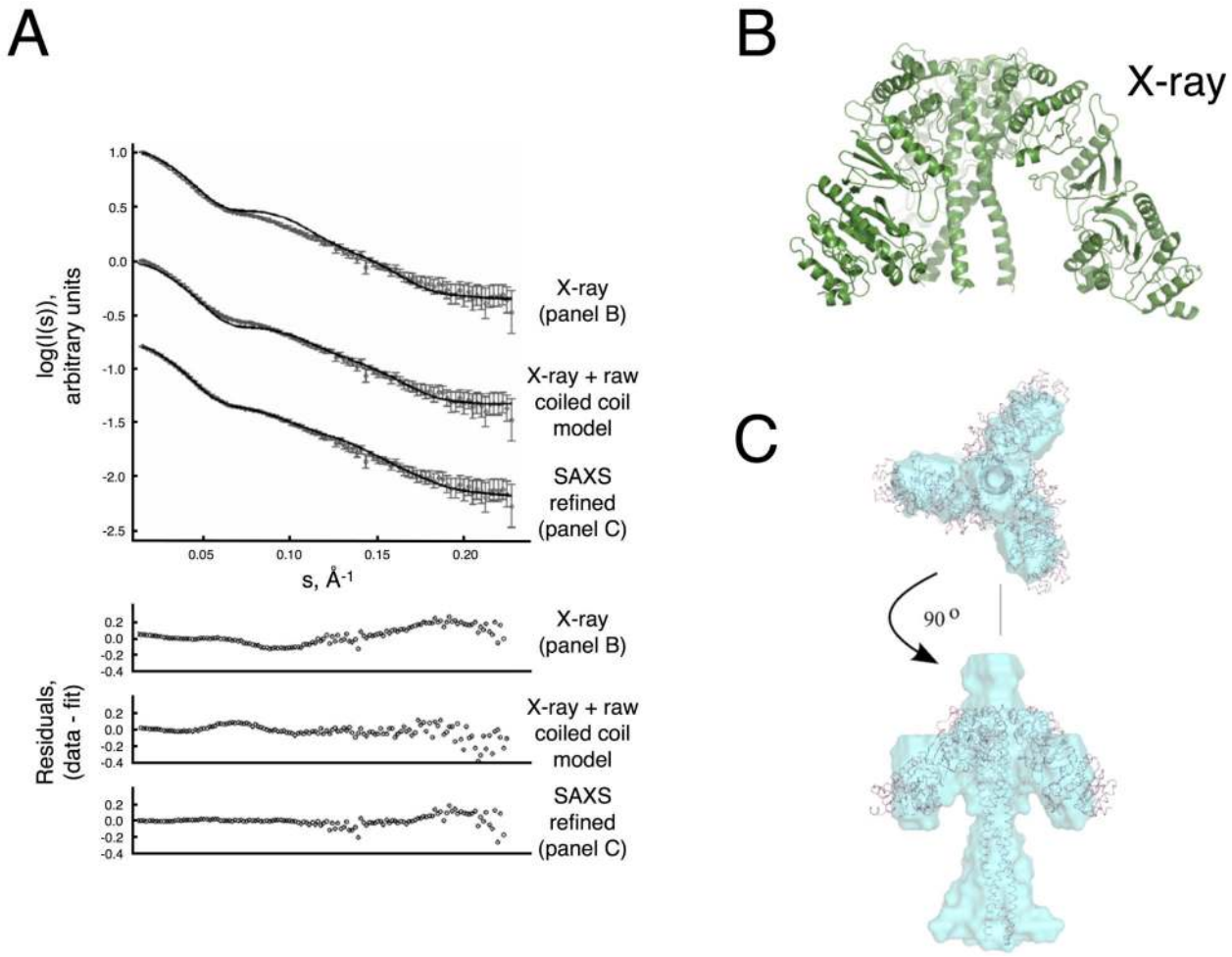

Figure 3.

A) Fits of different structural models (panels B,C) against the experimental WbdD$^{1\text{-}556}$ SAXS data (open circles with error bars representing standard deviations computed from propagated Poisson counting statistics) with the residuals of the fits shown below. **B)** Cartoon model of the new low-resolution structure with extended coiled-coil (same as in Figure 2A). **C)** *Ab initio* SAXS envelope of WbdD$^{1\text{-}556}$ (cyan) superposed with a model of WbdD $^{1\text{-}556}$ (purple) that was built as described in the main text and refined against the SAXS data.

Europe PMC Funders Author Manuscripts

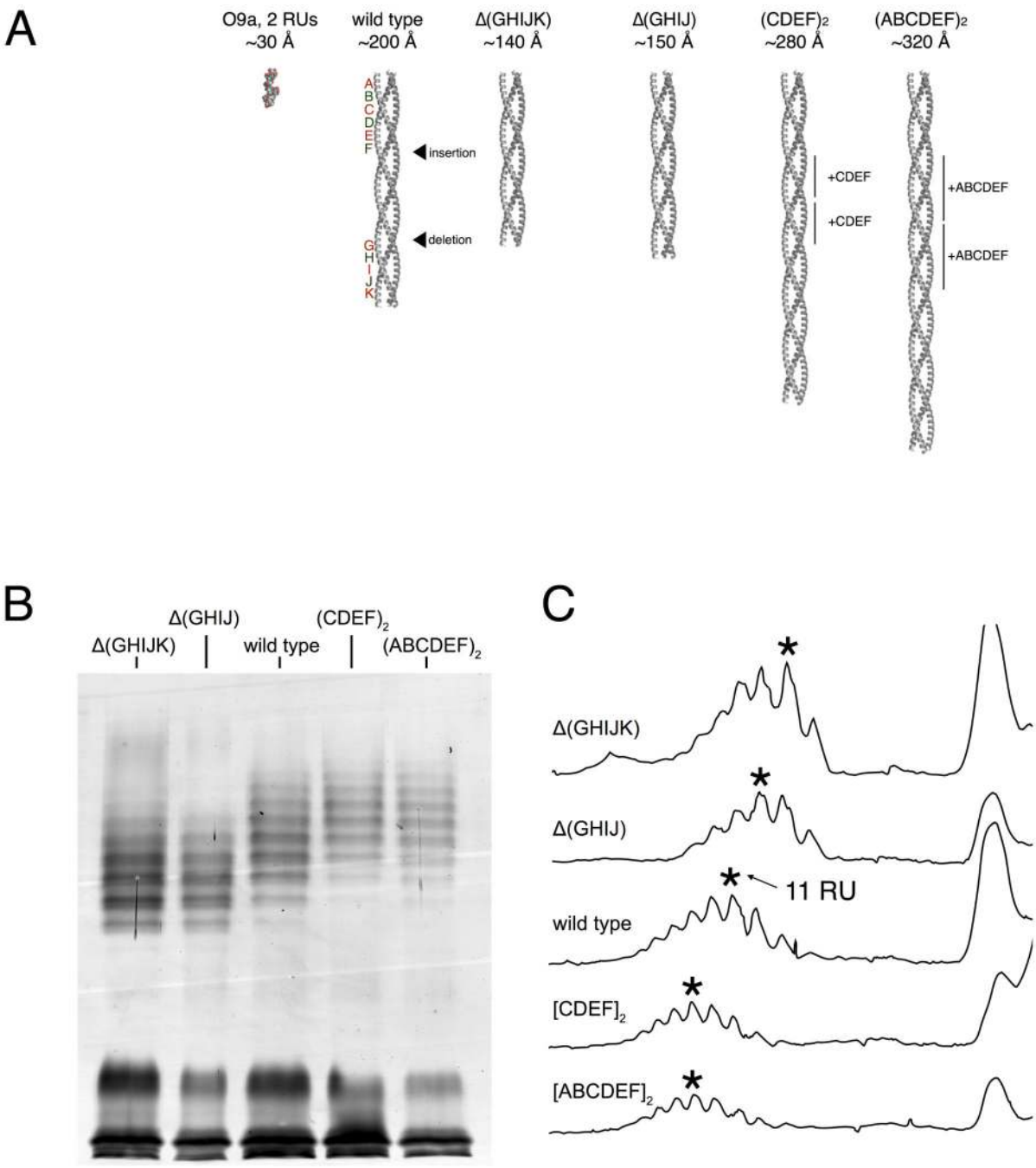

Figure 4.

A) Comparison of O9a LPS size distribution with lengths of the coiled-coil domains of different WbdD constructs in the experimental system. **B)** Silver stained SDS-PAGE of the LPS from WbdD wild type and the coiled-coil domain mutants shown in A). **C)** Intensity profiles of the gels shown in B). The profiles were calculated with ImageJ[42]. The maximum intensity band in each trace is marked by an asterisk.

Europe PMC Funders Author Manuscripts

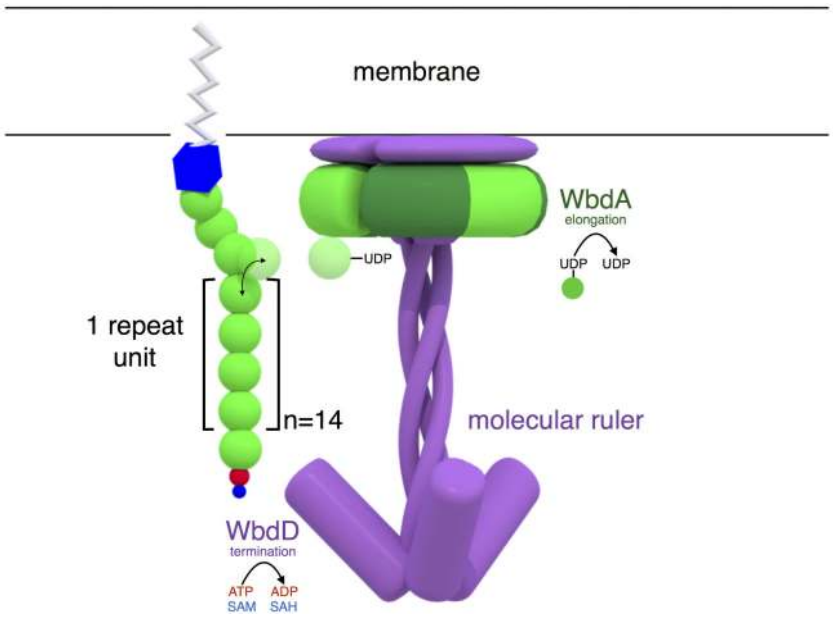

Figure 5.

Proposed model for elongation and termination of the O9a antigen. The membrane-attached polymer is extended (shown as translucent spheres, coloring as in Fig. 1B) by 3 copies of the multidomain WbdA polymerase (green ring). WbdA forms a complex with full length trimeric WbdD (which is anchored to the membrane, purple); note that the stoichiometry of the complex also influences the chain length[16]. As the polymer grows in length it will become long enough to reach the kinase active site of WbdD where polymerisation is terminated. The coiled-coil domain of WbdD separates the kinase from WbdA in space and thus is the essential element in the molecular ruler that regulates chain length of O-PS.

Europe PMC Funders Author Manuscripts

Table 1

Data collection and refinement statistics

	WbdD$^{1-556}$, PDB-ID: 4UW0
Data collection [1]	
Space group	I23
Cell dimensions	
a, *b*, *c* (Å)	181.3, 181.3, 181.3
α, *β*, *γ* (°)	90.0, 90.0, 90.0
Resolution (Å)	128.2-3.87 (4.0-3.87) *
R_{merge}	0.07 (0.59)
$I / \sigma I$	11.6 (2.3)
Completeness (%)	98.6 (99.3)
Redundancy	4.0 (3.7)
Refinement	
Resolution (Å)	128.2-3.87 (4.0-3.87)
No. reflections	8823
R_{work} / R_{free}	0.27 / 0.34
No. atoms	
Protein	4047
Ligand/ion	27
Water	0
B-factors (Å^2)	
Protein	171.5
Ligand/ion	126.8
Water	n/a
r.m.s. deviations	
Bond lengths (Å)	0.007
Bond angles (°)	1.301

* Values in parentheses are for highest-resolution shell.

[1] The reported data were collected from a single crystal.

Table 2

SAXS Data Collection and Scattering Derived Parameters.

Data collection parameters	**WbdD$^{1-459}$**	**WbdD$^{1-556}$**
Instrument	X33 (DORIS)	X33 (DORIS)
Beam geometry		
Wavelength (Å)	1.5	1.5
q-range (Å^{-1})	0.01-0.60	0.01-0.60
Exposure time (s)	15	15
Concentration range (mg ml^{-1})	1 - 10	1 – 5
Temperature (K)	283	283
Structural parameters *		
$I(0)$ (arbitrary units) (from $P(r)$)	47.5 ± 0.5	144.9 ± 0.5
R_g (Å) (from $P(r)$)	32 ± 3	53 ± 5
$I(0)$ (arbitrary units) (from Guinier)	47.4 ± 0.5	144.0 ± 0.5
R_g (Å) (from Guinier)	31 ± 3	52 ± 5
D_{max} (Å)	100 ± 5	170 ± 10
Porod volume (10^3 Å^3)	90 ± 10	380 ± 40
Dry volume calculated from sequence (10^{3}Å^3)	59.2	76.6
Molecular mass determination *		
MM_{POROD} (from Porod volume, kDa)	53 ± 5	220 ± 30
Contrast ($\Delta\rho \times 10^{10}$ cm^{-2})	3.047	3.047
MM_{saxs} (from $I(0)$, kDa)	52 ± 5	165±20
Calculated monomeric MM from sequence (kDa)	48.9	63.3

* Reported for infinite dilution of concentration series measurements